International Journal of Trend in Scientific Research and Development (IJTSRD)
Volume 10 Issue 3, May-Jun 2026 Available Online: www.ijtsrd.com e-ISSN: 2456 – 6470

Petrographical and Mineralogical Constraints on Fe-Ti-V Oxide Mineralizations Associated with the Doleritic dykes in the Téra-Ayorou Pluton (Liptako, West Niger)

Gambo Ranaou Noura[1], Abdou Dodo Bohari[2], Abdoulatif Abass Saley[3], Hassan Ibrahim Maharou[4], Ibrahim Sarki Laouali[5], Yacouba Ahmed[6]

[1,2,4,5,6]Faculty of Sciences and Technology, University of Abdou Moumouni, Groundwater and Georesources Laboratory, BP, Niamey, Niger
[3]School of Mines, Industry and Geology (EMIG), BP, Niamey, Niger

ABSTRACT

We examine the petrographical and mineralogical characteristics of Iron-Titanium-Vanadium oxide mineralizations associated with the doleritic dykes crosscutting the Téra-Ayorou pluton, located in the north of the Niger Liptako, which corresponds to the northeastern margin of the Léo-Man shield in the southern part of the West African Craton. These mineralizations are part of mineral resources discussed in this craton, but for which studies have been fragmentary and not known particularly in the Niger Liptako basement. The main of this study is to determine the metallogenic characteristics of these mineralizations through data collected in the field and processed in laboratory. Field data indicate that Fe-Ti-V oxide mineralizations of the Téra-Ayorou pluton are associated with hematite, in the form of iron oxides, and formed during surface weathering. Thin sections, EDS and SEM maps demonstrated that these mineralizations occur as Fe-Ti-V oxides in titanomagnetite with ilmenite exsolutions, in titanomaghemite, and in metal sulfides and some silicate minerals such as clinopyroxenes, hornblende, chlorite, and the emplacement mechanism suggest formation essentially during magma evolution. Electron microprobe analyses data indicate high concentrations in TiO_2 (21.61–50.51 wt%), FeO (3.47–67.16 wt%), and low V_2O_5 (0.001–0.005 wt%) for the oxidized minerals, and suggest several sources, notably fractional crystallization, deuteric oxidation and hydrothermal alteration. These mineralizations are associated with high Ca and S content in titanomagnetite and sulfides respectively and minor Mn and Cr contents in titanomaghemite and clinopyroxene respectively. Its occur as disseminated in these dykes and originate from lithospheric mantle and formed in magma chamber.

How to cite this paper: Gambo Ranaou Noura | Abdou Dodo Bohari | Abdoulatif Abass Saley | Hassan Ibrahim Maharou | Ibrahim Sarki Laouali | Yacouba Ahmed "Petrographical and Mineralogical Constraints on Fe-Ti-V Oxide Mineralizations Associated with the Doleritic dykes in the Téra-Ayorou Pluton (Liptako, West Niger)" Published in International Journal of Trend in Scientific Research and Development (ijtsrd), ISSN: 2456-6470, Volume-10 | Issue-3, June 2026, pp.906-922, URL: www.ijtsrd.com/papers/ijtsrd125018.pdf

IJTSRD125018

KEYWORDS: *Fe-Ti-V oxides, mineralizations, doleritic, dykes, Téra-Ayorou, Liptako.*

1. INTRODUCTION

Fe-Ti-V oxide mineralizations are commonly associated with opaque and sulfide minerals such as hematite, sulfides, spinel, ilmenite, magnetite. These types of mineralizations are the subject of extensive research worldwide due to their economic importance and their technological and infrastructure applications. Its occur as disseminated oxides in silicate rocks or as massive oxides in dykes, sills, or lenses (Pang et al., 2010). Several metallogenic studies have demonstrated that Fe-Ti-V mineralizations can be associated with mafic-ultramafic intrusions (e.g., Jiang et al., 2024; Latypov et al., 2024), gabbroic/anorthositic complexes (e.g., Charlier et al., 2015; Khalil et al., 2023; Khedr et al., 2022), ophiolitic complexes (Falaknazi and Karimi, 2014), gneissic complexes (Mohammad et al., 2022), carbonatites (Uwamungu et al., 2023), and flood basalts associated with Large Volcanic Provinces (e.g., Song et al., 2013; Cao et al., 2019). These mineralizations may have a magmatic origin (Karinen

et al., 2022), i.e., formed through magma differentiation (Zhou et al., 2013; Jonsson et al., 2013; Bai et al., 2019), post-magmatic process (such as hydrothermal alteration, Li et al., 2014; Dare et al., 2014) or supergene alteration (related to fluvial weathering, Weibel, 2003). Most studies have shown that Fe-Ti-V oxide mineralizations associated with mafic-ultramafic intrusions and anorthosite/gabbro complexes are the most widely studied worldwide.

In the West African Craton, earlier metallogenic studies have compiled a regional inventory demonstrating the spatial distribution of gold, sulfide, iron, vanadium, rare earth, titanium, platinum group elements (PGEs), phosphate, tungsten, nickel, manganese, mercury, aluminum, gem, molybdenum, chromium in this craton (Markwitz et al., 2016, Aïfa, 2021; Baratoux et al., 2024); however, most of its have focused on gold mineralizations and associated substances (e.g., Béziat et al., 2008; White et al., 2014; Sangaré et al., 2014; Ballo et al., 2015; Noura et al., 2024). With the exception of studies carried out on large ultramafic intrusion-hosted Fe-Ti-V deposits in Guinea (Gluaguen et al., 2015), no study has specifically focused on these mineralizations to date. These types of mineralization, although associated essentially with tholeiitic host rocks, which are potential sources, remain little known or poorly understood, even though a significant mafic-ultramafic rocks associated with the greenstone belts in this craton are tholeiitic in nature.

In the Niger Liptako region, and in the Téra-Ayorou pluton in particular, research work on Fe-Ti-V mineralizations are also not conducted to date. The metallogenic studies are undertaken on gold, copper, molybdenum, rare earth elements (Nb, Ta, Mo, Li), manganese, and chromium (Machens, 1973; Attourabi et al., 2024b; Garba Saley et al., 2024; Noura et al., 2024). This work will attempt to provide new data on these types of mineralization, especially as the work of Noura et al. (2023a, 2025) have demonstrated the presence of significant proportion of oxyde minerals in the doleritic dykes of the Niger Liptako region. The main of this publication is to determine the metallogenic characteristics of Fe-Ti-V oxide mineralizations associated with the doleritic dykes crosscutting the Téra-Ayorou pluton, by using petrographic and mineralogical approachs.

2. Geological setting

The West African Craton is a tectono-magmatic and metamorphic structure that has undergone three orogenic events, notably the Leonian (3.2–2.9 Ga, e.g., Koumelan et al., 2018; Grenholm et al., 2019), the Liberian (2.9–2.5 Ga, e.g., Thieblement et al., 2004; Grenholm et al., 2019), and the Eburnean (2.3–2.0 Ga, e.g., Soumaila et al., 2008; Vidal et al., 2009; Baratoux et al., 2011; Parra-Avila et al., 2017), which allowed for the definition of its current configuration following a stabilization period estimated between 1.8 and 1.6 Ga (Ennih and Liégeois, 2008; Lompo, 2009). It consists of two shields: (*i*) the Réguibat shield to the north and (*ii*) the Leo-Man shield to the south, separated by the Taoudenni Basin in the center. The two shield are similar and comprise an Archean province to the west and a Birimian province to the east. The Archean provinces consist of rocks typically emplaced during the Leonian and Liberian orogenic events, whereas the Birimian provinces are composed of rocks formed during the Eburnean orogeny. The Birimian rocks of the Leo-Man shield consist of greenstone belts, intersecting by granitoid batholiths (Figure 1). These two rocks were crosscut by mafic sills and dykes, whose spatial distribution-spanning less than 200 m in thickness over lengths ranging from 300 to 1,000 km is shown on the aeromagnetic map of Jessell et al. (2015), modified by Baratoux et al. (2019) and Noura et al. (2023a). These authors have highlighted the existence of more than 3,000 dykes grouped into 26 swarm types based on their orientations, while radiometric studies have indicated approximately 10 generations of mafic dykes in the Birimian domain, which ages range from 1.79 to 0.55 Ga (e.g., Youbi et al., 2011; Jessell et al., 2015; Baratoux et al., 2019; Noura et al., 2023a).

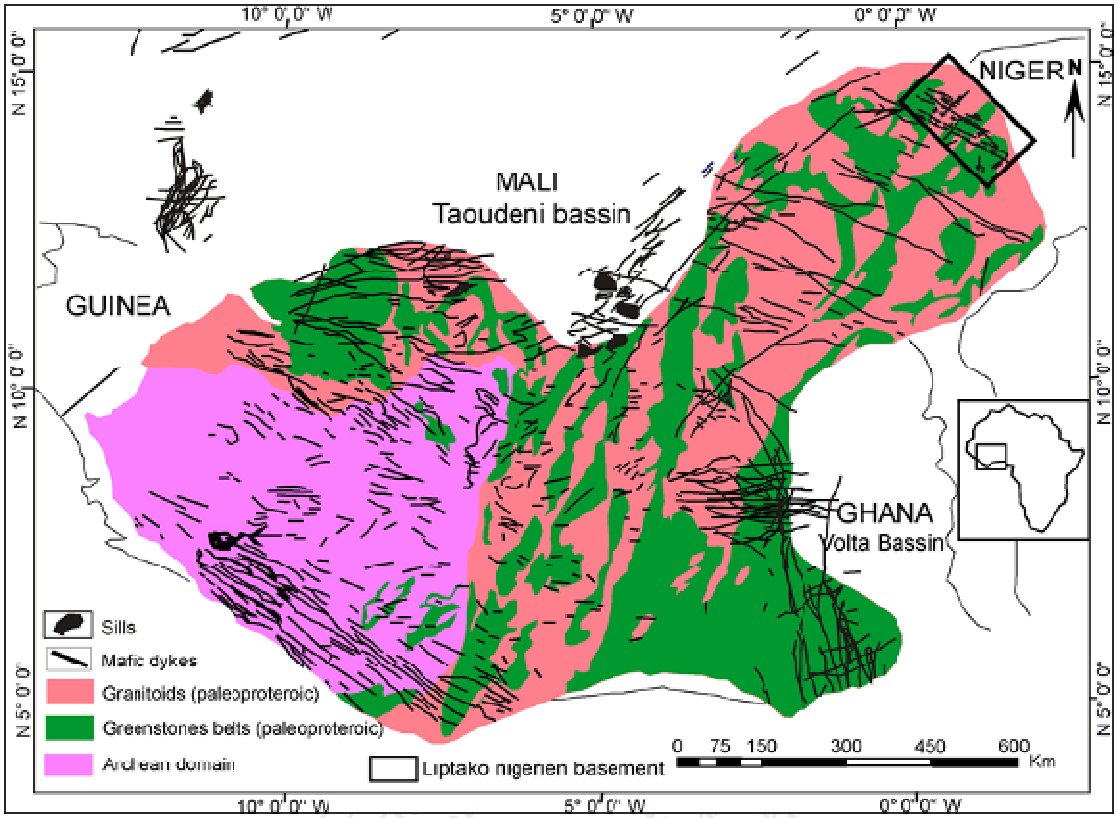

Figure 1: Geological map of the Leo-Man Shield with associated sills and mafic dykes after Jessell et al. (2015), modified by Baratoux et al. (2019), and Noura et al. (2023a).

The Niger Liptako corresponds to the NE end of the Baoulé-Mossi domain of the Leo-Man Ridge (Figure 2). The basement of the Nigerien Liptako consists of alternating belts of greenstone, notably the Gorouol, Diagorou-Darbani, Sirba, and Makalondi belts, and granitoid plutons, namely the Téra-Ayorou, Dargol-Gotheye, and Torodi plutons, arranged spatially in a NE-SW direction. Several studies (e.g., Machens, 1973; Dupuis et al., 1991; Pons et al., 1995; Ama Salah et al., 1996; Soumaila et al., 2016b; Hallarou et al., 2020b; Ahmed et al., 2022; Attourabi et al., 2024b; Garba Saley et al., 2024; Noura et al., 2025) have noted that these two groups consist of basic (basalts, gabbros, dolerites), intermediate (tonalites, trondhjemites, granodiorites, diorites, dacites), and acidic (rhyolites, granites, syenites), as well as metamorphic (pyroxenites, amphibolo-pyroxenites, serpentinites, schists, phyllites, gneisses, migmatites, grauwackes) and volcano-sedimentary (tuffs, cinerites) rocks. All of these formations are cut by pegmatite, quartzite, and aplite veins, as well as doleritic dykes, running in various directions (e.g., Pons et al., 1995; Attourabi et al., 2024b; Noura et al., 2025), with a concentration of doleritic dykes north of the Téra-Ayorou pluton (Figure 3). Precambrian sedimentary sequences (carbonates, sandstones, diamictites, e.g., Ibrahim Maharou et al., 2024a), Oligocene of Terminal Continental 3 (clayey sandstone, oolites; e.g., Ousmane et al., 2020) and Quaternary (sand dunes) lie in major unconformity on the basement formations.

Cartographic studies have shown that the doleritic dikes of the Liptako are oriented arbitrarily along four major directions, notably N-S, WNW-ESE, NW-SE, and E-W (Noura et al., 2023a; Noura et al., 2025). Geochemical studies have demonstrated a continental basalt affinity for all these dikes, but divided into two distinct basaltic series, notably oceanic plateau basalts for the WNW-ESE to NW-SE-trending dykes (Noura et al., 2023a), and calc-alkaline basalts for the N-S-trending dykes (Noura et al., 2025). The dykes of WNW-ESE, NW-SE, and E-W-trending are the focus of this study and account for approximately 80% of the intrusive dykes, and located in the northern part of the Liptako region. Radiometric studies have dated one N135°-trending dyke at 896 Ma (K/Ar age, Ama Salah, 1991), which is considered as their emplacement age. In contrast, the N-S dykes yielded three K/Ar ages ranging from 1.37 to 1.01 Ga (Ama Salah, 1991) and a U/Pb age of 1.79 Ga (Baratoux et al., 2019).

Metallogenic studies have shown that the mineralizations studied in the Niger Liptako are predominantly associated with greenstone belts and are represented by gold (Machens, 1973; Abass Saley et al., 2021; Noura et al., 2024); copper and molybdenum (Machens, 1973; Hallarou et al., 2020b); chromium and manganese (Machens, 1973; Garba Saley et al., 2024), and rare earth elements (Machens, 1973; Attourabi et al., 2024b).

The mechanism and setting for the formation of these mineralizations proposed these authors consist of circulation of hydrothermal fluids rich in metallic substances, which deposit it in fractures and brittle shear zones.

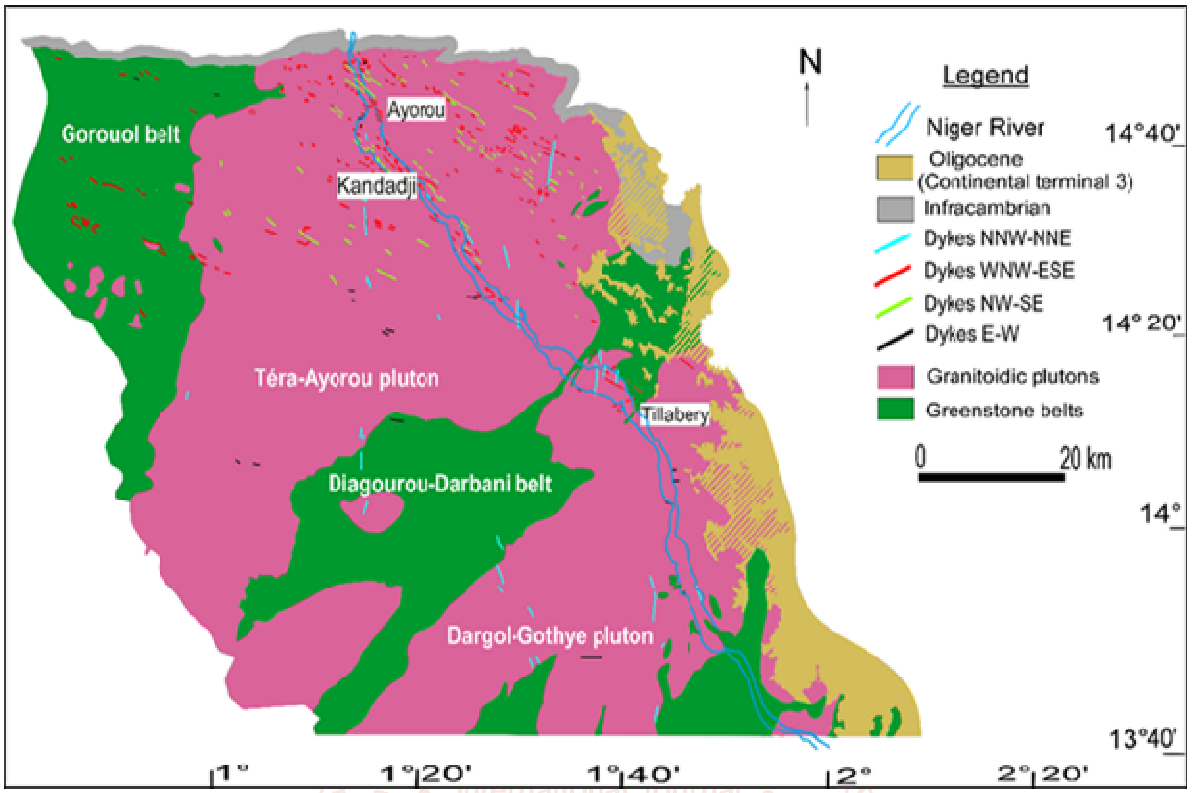

Figure 2: Extrated from the geological map of the Niger Liptako basement (Machens, 1973).

2.1. Geological setting of the Téra-Ayorou pluton

The Téra-Ayorou pluton (Figure 3) is located in the north-central part of the Niger Liptako. This pluton consists of foliated granodiorite, which accounts for more than 70% of the total volume of granitoids in the pluton (Pons et al., 1995), single- and two-mica granites, and migmatites (Machens, 1973; Pons et al., 1995; Attourabi et al., 2024b). Foliated granodiorite is characterized by circular foliation in the center of the pluton and generally NE-SW-trending foliation at the pluton margins (Soumaila and Konaté, 2005; Ahmed et al., 2022; Noura et al., 2023b). Foliated granodiorite is crosscuted by porphyritic granodiorite and quartzite diorites and syenites (Pons et al., 1995; Ahmed et al., 2022; Attourabi et al., 2024b; Noura et al., 2023b) in the form of intrusive bodies of varying sizes. Dykes oriented WNW-ESE, NW-SE, and E-W outcrop as aligned blocks stained by a reddish or blackish surface layer formed during the surface weathering. Crystal size in the doleritic dykes varies between the cores, where grains are fine to medium, and the chilled margins, where grains are fine. The structural classification used by Noura et al. (2023a) indicated that the WNW-ESE dykes are oriented between N110° and N120°, the NW-SE dykes between N130° and N140° and the E-W between N90° and N100°. These dykes account for approximately 80% of the intrusive dykes in the Liptako and consist of an assemblage of mafic minerals (augite, ferroedenite, biotite), oxidized minerals (titanomagnetite), and plagioclase, apatite, and chlorite (Noura et al., 2023a). They are affected by deuteric alteration, which cause the transformation of pyroxene into ferroedenite, biotite into chlorite, and plagioclase into sericite (Noura et al., 2023a). The geochemical study demonstrated that they have an asthenospheric origin and these magma was formed by partial melting of a spinel-bearing lherzolite containing residual garnet (Noura et al., 2023a). From a structural perspective (Tourba et al., 2024), the doleritic dykes of the Téra-Ayorou pluton are characterized by a brittle deformation phase, subdivided into two episodes. Episode D1, responsible for normal faults and fractures N70° to N110°-trending, is linked to N-S extension, whereas episode D2, responsible for brittle shear zones and fractures oriented between N150° and N170°, is associated with ENE-WSW extension.

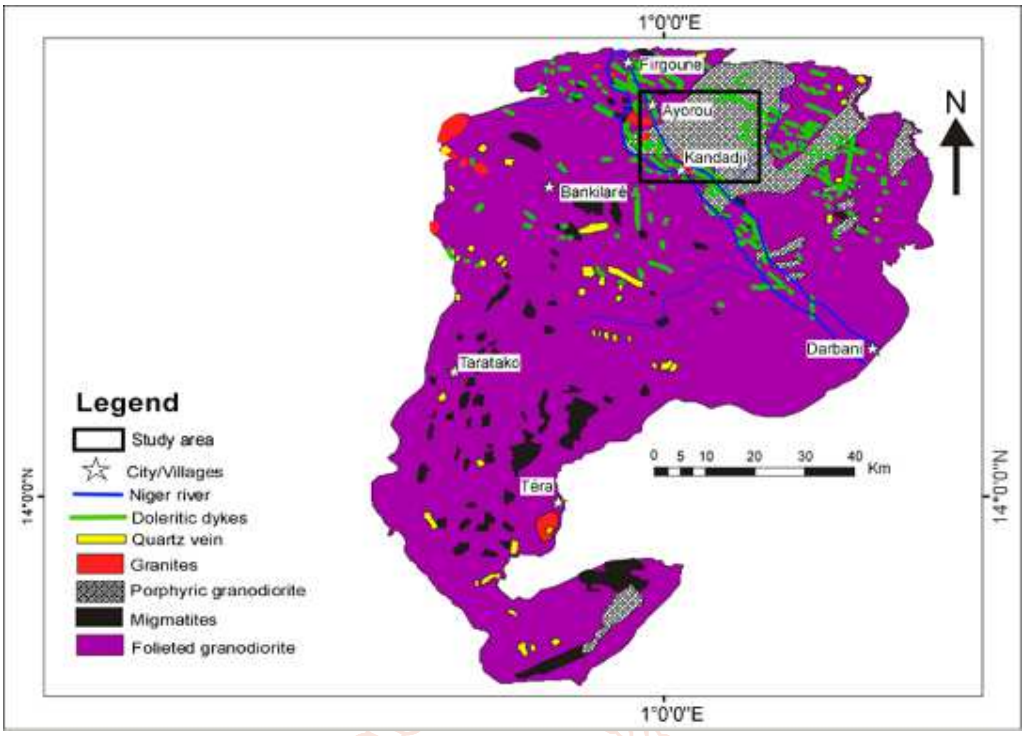

Figure 3: Geological map of the Téra-Ayorou pluton (extrated from Figure 2, Machens, 1973).

3. Methodology

The methodology employed in this study consisted of collecting samples in the field and their processing in the laboratory. During sampling, fresh and weathered samples were collected from the cores and chilled margins of doleritic dykes to understand the effects of supergene weathering and magma différenciation. Laboratory work included microprobe analysis, energy-dispersive spectroscopy (EDS), and chemical cartography. Microprobe analysis, energy-dispersive spectroscopy and chemical mapping were performed at the GET Laboratory at the University of Toulouse in France. Microprobe analysis and chemical mapping focused on oxides, while energy-dispersive spectroscopy additionally focused on sulfides. More than 10 points were analyzed and mapped on each crystal to know possible chemical variations and to map the texture of the oxide and sulfide minerals. Energy-dispersive spectroscopy was performed on the DAF1 dyke sampled at Ayorou and oriented N90° and the KD3 dyke sampled at Kandadji and oriented N120°. Microprobe analysis and chemical mapping were conducted on three samples, represented by DAN3, collected at Ayorou from a N120°-trending dykes, DSA3, sampled at Ayorou from a N130° -trending dykes, and KD4, collected at Kandadji from a N110°-trending dykes. The characteristics (symbols, orientations, sampling coordinates) of these sampled dykes in our study area are listed in Table 1. The petrographic and mineralogical characterizations will focus essentially on oxidized and sulfide minerals, the main hosts of Fe-Ti-V mineralization and given that the silicate minerals have been sufficiently studied in Noura et al. (2023a).

The instrument used for the mineralogical analysis and chemical mapping is a Tescan Vega 4 LMU scanning electron microscope, coupled with a Bruker Quantax 30 mm² SDD EDX detector. The operating voltage is 15 kV. The working distance and pixel size range from 10 to 16 mm and 50 to 70 µm, respectively, while the magnification ranges from 5 to 1000x.

Tableau 1: Characteristics of doleritic dykes sampled in the Téra-Ayorou pluton.

Symbols of dykes	Specific trends	Majors arbitrary trends	Lat. N	Long. E
DAF4	N110°	WNW-ESE	14.729	0.914
DNA2	N115°		14.712	0.923
KD4	N110°		14.602	1.015
DNA3	N120°		14.751	0.984
DNA5	N140°-	NW-SE	14.744	0.910
DAF2	N140°		14.505	0.911
DSA3	N130°		14.719	0.917
DAF1	N090°	E-W	14.750	0.908
DSA2	N100°		14.718	0.9191

4. Results

4.1. Petrographic characteristics of Fe-Ti oxide minerals

The field petrographic study conducted in boths sectors indicate that the dikes outcrops as fragmented blocks in the dyke centers and locally in contact with the host rocks at the chilled margins. The identified minerals are superficiel oxides and sulfides. Oxides are observed everywhere, on the fragmented blocks at the centers of the dikes (Figure 4c), on their chilled margins (Figure 4b), and on centimeter-thick veins of dolerites (Figures 4a, 4d), in the form of a weathering patina. This patina forms during superficiel weathering and consists of hematite. The patina is characterized by a rust-colored hue in the center of the dykes and a slightly blackish one at their chilled margins (Figure 4). It is formed by the action of water on the ferro-magnesian minerals during the oxidation of Fe contained in the clinopyroxenes. It is massive and exhibits a metallic luster with irregular fractures at the chilled margins (Figure 4d). Sulfides occur locally in the fresh parts as small, sub-morphic crystals of bright yellow color and millimeter size.

Figure 4: Photographs showing surface-oxidized minerals on outcrops of doleritic dykes in the Téra-Ayorou pluton.

Analysis of thin sections under polarized light revealed the physical characteristics of the oxidized and sulfide minerals hosting Fe-Ti-V mineralization. The oxidized minerals are characterized in all thin sections by brownish xenomorphic crystals in the form of granular aggregates of titanomagnetite, intergrown with fine grains of ulvospinel and/or bands of ilmenite (Figure 5). These features are typical of the lattice texture of titanomagnetite (Figure 5c, e). Fine spinel inclusions occur locally, while lamellae and granules are present in all thin sections. Titanomagnetite granules account for approximately 60% and measure no less than 400 µm in all dykes, while fine granular inclusions of ulvospinel and ilmenite lamellae account for less than 5% and 30%, respectively, with dimensions smaller than 400 µm. The titanomagnetite crystals stand out in relief against the deeply altered clinopyroxene and plagioclase crystals and the fibrous crystals of late- to post-magmatic minerals, notably hornblende and chlorite, which are identified at the margins of the clinopyroxene. The lamellae appear as hexagonal bands that are more or less parallel or intersecting with one another, thus forming the ilmenite spearhead twinning (Figure 5c). This texture is related to the separation of iron and titanium during the recrystallization of ilmenite from titanomagnetite. In some thin sections, a transformation of titanomagnetite into titanomaghemite is observed (Figures 5d, 5e, 5f). The latter is characterized by xenomorphic crystals, often discolored, within which a few remnants of ilmenite still persist.

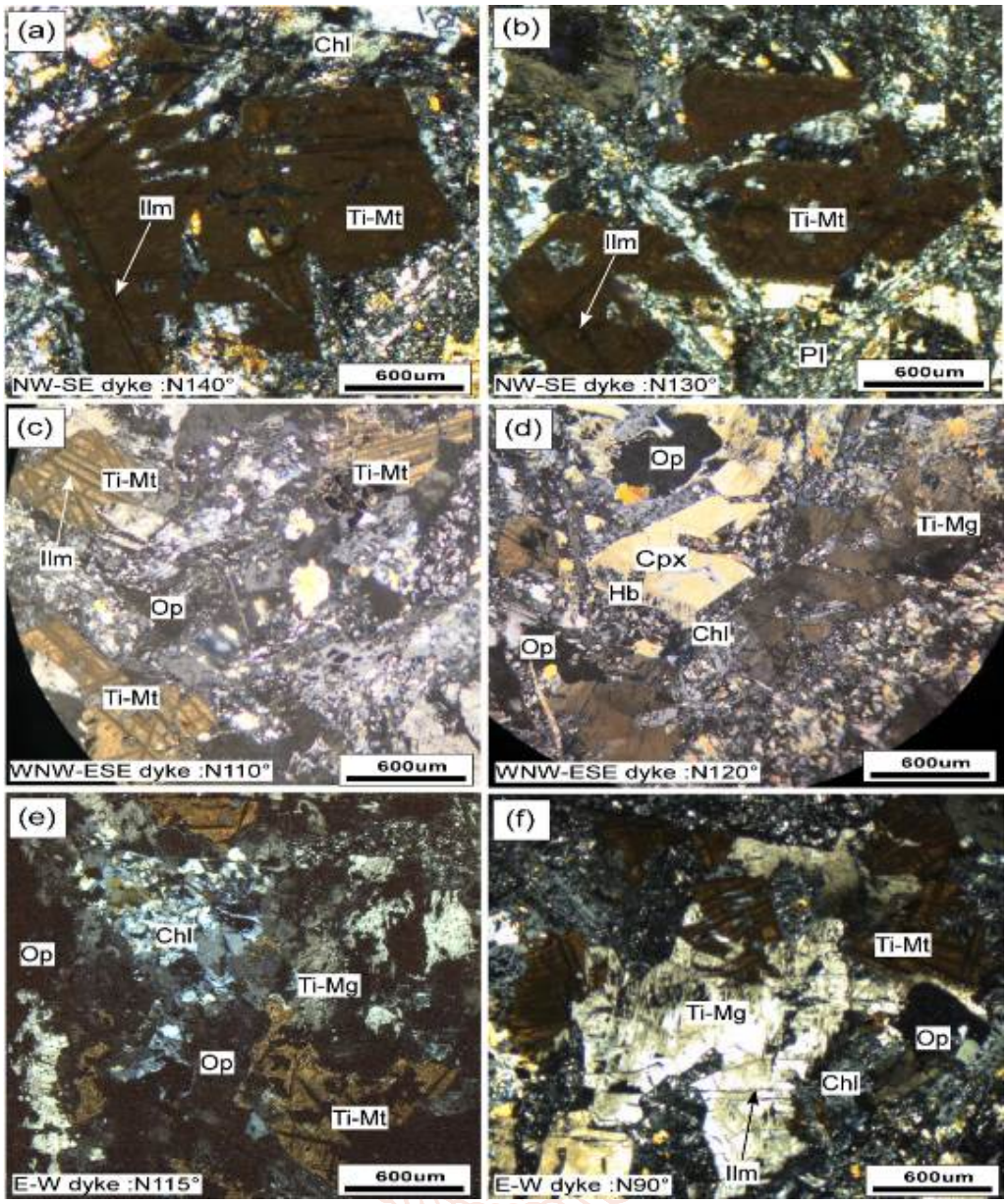

Figure 5: Microphotographs showing the altered texture by deuteric oxydation or alteration and mineralogical composition of oxidized minerals present in the doleritic dykes of the Téra-Ayorou pluton. Cpx: clinopyroxene, Pl: plagioclase. Chl: chlorite, Ti-Mt: titanomagnetite, Ti-Mg: titanomaghemite, Op: opaque, Ilm: ilmenite.

4.2. Mineralogical characteristics of Fe-Ti-V oxide mineralizations

Analysis of SEM images and observation EDS spectra from dyke DAF1 (Figure 6a, b) provide additional details on the petrographic characteristics of the Fe-Ti-V oxide mineralizations in our study area. The observations indicate the same types of minerals (titanomagnetite, plagioclase, clinopyroxene) and the additional presence of pyrite (Figure 6a). The spectra are characterized by high peaks of sulfur (derived from pyrite and detectable up to approximately 400 counts/eV) and silicon (derived from silicate minerals and detectable up to approximately 140 counts). Other elements (Ca, Ti, Fe, Al), present in all minerals described above, are detectable between 70 and 170 counts/eV and characterized by moderate to weak peaks of these elements. The results demonstrate that these mineralizations are associated with sulfur (S) and calcium (Ca). The results obtained for the KD4 dyke (Figure 6c, d) differ in part from those of the DAF1 dyke, due to the presence of chalcopyrite, titanomaghemite, and significant peaks in S and Ti. Similarly, the titanomagnetite crystals are characterized by a typical lamellar texture with banded intergrowth of ilmenite and partial transformation into titanomaghemite. In addition, new chemical elements appear, notably Cu (detectable up to approximately 100 counts/eV and present in chalcopyrite, Figure 6c) and Mn (detectable up to approximately 40 counts/eV and present in ilmenite and/or titanomaghemite, Figure 6d). The presence of these minerals confirms that the Fe-Ti-V oxide mineralizations of our study area are also associated with metal sulfides.

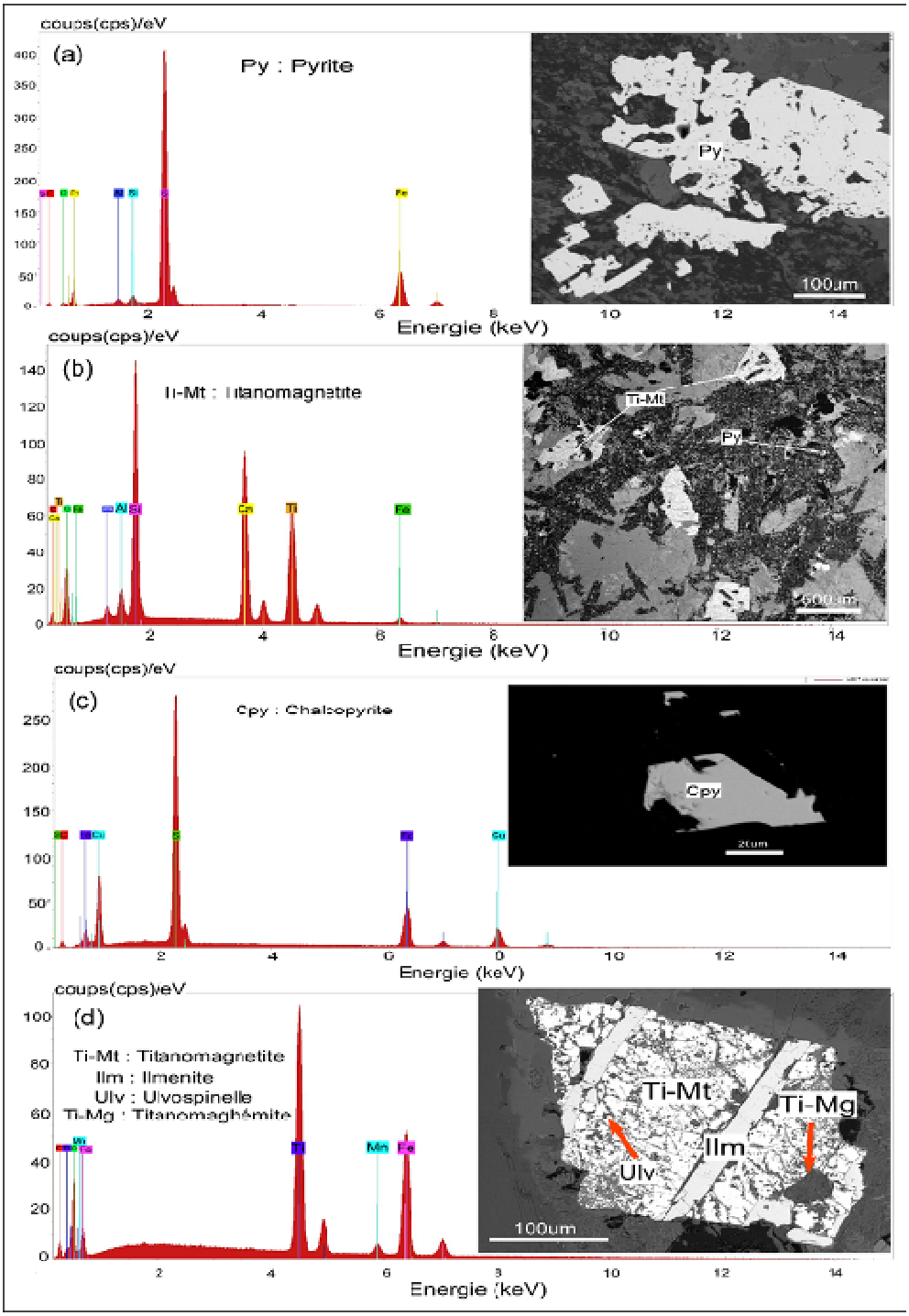

Figure 6: SEM maps and EDS spectra of the KD4 (a and b) and DAF1 (c and d) dykes. In (a) chalcopyrite is visible, in (b and d) titanomagnetite, and in (c) pyrite. Cpy: chalcopyrite, Py: pyrite, Ti-Mg: titanomagnetite, Cpx: clinopyroxene, Pl: plagioclase, Ti-Mt: titanomagnetite.

To examine the physical characteristics and distribution of Fe-Ti-V and other associated elements within the crystals observed earlier, chemical maps and SEM images of certain elements (Ca, Ti, Fe, Mn, Si) were used (Figure 7). The distribution of elements within the crystals allows for more identification of the texture and nature of the minerals and even for estimating the percentage of each element. Based on the colors assigned to the elements, ilmenite is characterized by a high concentration (over 45%) of Fe and Ti and distinct lamellar intergrowth within the titanomagnetite, which contains less than 35% of these elements. The presence of Ca is observed in approximately 20% of the titanomagnetite, demonstrating that it is vanadiferous in nature, unlike ilmenite, which does not show the presence of this element (Figure 7b). The intensity of Mn (Figure 7e) compared to Fe or Ti (Figure 7g) demonstrates that it is present in trace amounts in ilmenite and titanomaghemite. Based on the Mg–Fe–Ti association, it is evident that ilmenite-banded titanomagnetite is the primary mineral hosting Fe–Ti–V oxide mineralization and is transformed into titanomaghemite in some dykes.

The silicate minerals, identified by the distribution of Si on chemical maps (Figure 7f) or the Ca–Mg combination on SEM images (Figure 7g, h), correspond to clinopyroxene and plagioclase. The distribution of chemical elements demonstrates that the predominant mineralizations in titanomagnetite are Fe–Ti–V associated with Ca (Figure 7). It is noted that Fe–Ti oxides are slightly associated with traces such as Mn in ilmenite, compared to titanomagnetite (Figure 7g, h). Furthermore, a relatively high concentration of Fe is observed at the margins of clinopyroxene crystals bordering chlorite or hornblende. Titanomaghemite contains the same elements (Fe, Ti) as titanomagnetite, in addition to Mn in titanomaghemite (Figure 8g). The presence of Fe, Ti, and Mn in hornblende, chlorite, and titanomagnetite indicates a contribution of weathering to the formation of these mineralizations. Thus, the Fe–Ti–V oxide mineralization in our study area occurs in a primary stage in titanomagnetite and sulfides, in a late-magmatic stage in titanomaghemite and hornblende; and in a post-magmatic stage in chlorite.

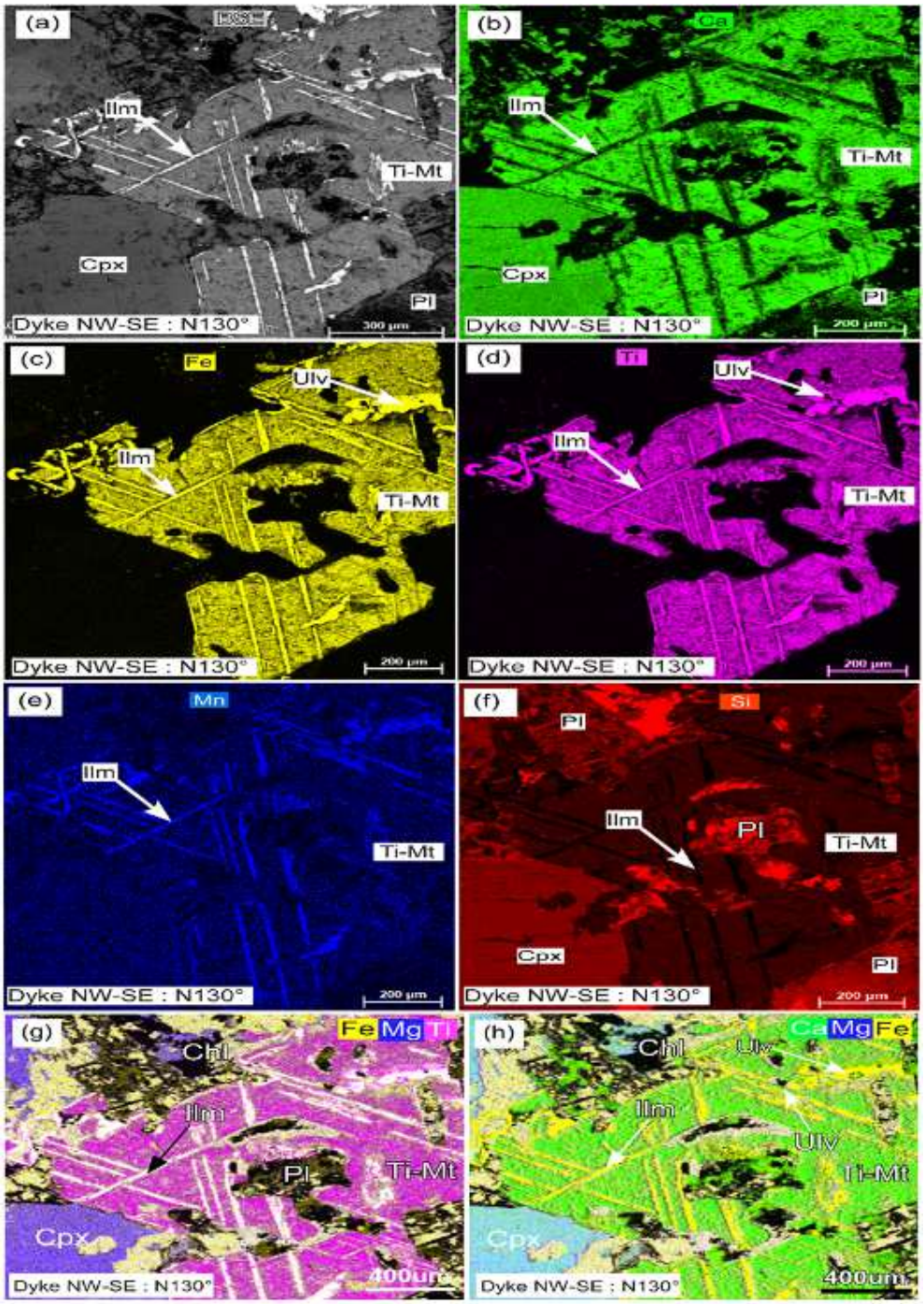

Figure 7: (b, c, d, e, f). Chemical maps showing the spatial distribution of (b) calcium, (c) iron, (d) titanium, (e) manganese, and (f) silicium in the oxyde minerals. (a, g, h) show SEM images illustrating the combination of chemical elements. Cpx: clinopyroxene, Pl: plagioclase. Chl: chlorite, Ti-Mt: titanomagnetite. Ilm: ilmenite, Ulv: ulvospinel.

The electron microprobe analysis made it possible to determine the nature of the oxidized minerals more precisely and to ascertain the percentages of Fe-Ti-V oxides (Table 2). The results show that these mineralizations are characterized by high contents of TiO2 (21.61–50.51 wt%), and FeO (3.47–67.16 wt%), moderate contents of CaO (0.020–24.96 wt%) and SiO_2 (26.36–29.69 wt%), and relatively low contents of Cr_2O_3 (0.020–0.070 wt%) and MnO (0.04–3.71 wt%). The relatively high TiO_2 (21.61–50.51 wt%) and FeO (43.10–67.16 wt%) and low MnO (0.04–3.71 wt%) contents are represented by ilmenite and ulvospinel. Titanomagnetite is characterized by high TiO_2 (31.08–33.22 wt%), FeO (10.03–12.92 wt%) and CaO (23.98–24.04 wt%) and low in MnO (0.04–0.50 wt%) contents, unlike titanomaghemite, which shows a decrease in FeO (3.47 wt%) and a relative increase in the proportions of TiO_2 (35.10 wt%) and MnO (3.002 wt%). The relatively high contents of Ca (23.980–24.960 wt%) are related to the vanadiferous nature of titanomagnetite. Magnetite is commun analyzedminerld mineral based on two oxides observed in plagioclase laths, contains high FeO contents (61.31–61.32 wt%) out of a total well below 100, and low V contents (V_2O_5: 0.001–0.005 wt%). However, geochemical analyses of bulk rocks (Noura et al., 2023a) indicate that the V contents of these dykes range from 316 to 505 ppm. The plotting of the electron microprobe analysis results for the oxides analyzed in the dykes of this study on the FeO – Fe_2O_3 – TiO_2 diagram (Deer et al., 1969) demonstrates the positioning of samples above the solvus of three oxide series: (i) the pseudobrookite series (ferropseudobrookite–pseudobrookite), (ii) the titanohematite series (ilmenite-hematite), and (iii) the titanomagnetite series (ulvospinel-magnetite). The proximity of the samples to the stability lines defining the three oxide series can be explained by the evolution of the magma during deuteric oxidation. For example, samples projected above the titanomagnetite solvus also share the stability field of titanomaghemite, which is a product of deuteric oxidation alteration of titanomagnetite (Figure 8). These observations indicate the presence of Fe-Ti-V oxide mineralizations in the dykes of our study area in various stages, notably (i) the primary origin, (ii) the late magmatic stage, and (iii) the post-magmatic remobilisation. These process could include fractional crystallization, deuteric alteration and oxidation, hydrothermal alteration, or post-magmatic metamorphism alteration.

Table 2: Representative electron microprobe analysis resultats of Fe-Ti-V oxides minerals (wt.%) of Ayorou and Kandadji sectors. Mt: Magnétite, Ti-Mt: Titanomagnetite, Ti-Mg: Titanomaghémite, Ilm: Ilménite, Ulspl: Ulvospinelle. Analysis results of samples KD4a and DSA3c are from Noura et al. (2023a).

Samples Minerals	KD4a Ilm	KD4bù§ Ilm	DSA3a Ti-Mt	DSA32b Ti-Mt	DSA3c Ulspl	DNA3a Ilm	DNA3b Ti-Mg
MgO	0.020	0.000	0.000	0.690	0.030	0.000	1.160
Al_2O_3	0.000	0.000	1.250	2.760	1.380	0.050	2.220
SiO_2	0.010	0.020	26.360	27.810	0.720	0.050	29.690
CaO	0.030	0.240	24.040	23.980	0.710	0.370	24.960
TiO_2	50.450	50.050	33.220	31.080	21.610	50.510	35.100
Cr_2O_3	0.020	0.000	0.050	0.070	0.050	0.030	0.060
V_2O_5	0.005	0.003	0.000	0.002	0.002	0.009	0.000
MnO	3.560	3.710	0.040	0.050	0.040	2.950	3.802
FeO	43.590	43.060	12.920	10.030	67.160	43.100	3.470
Fe_2O_3	47.555	46.966	14.359	11.147	74.638	48.010	3.856
Sum	100.700	100.019	99.319	97.589	99.180	100.979	100.888
Mg	0.001	0.000	0.000	0.021	0.001	0.000	0.035
Al	0.000	0.000	0.030	0.067	0.040	0.001	0.053
Si	0.000	0.000	0.538	0.569	0.018	0.001	0.598
Ca	0.001	0.006	0.526	0.525	0.019	0.009	0.538
Fe^{2+}	0.962	0.956	0.229	0.177	1.803	0.954	0.059
Ti	0.978	0.977	0.530	0.492	0.522	0.983	0.537
Cr	0.000	0.000	0.001	0.001	0.001	0.001	0.001
V^{5+}	0.000	0.000	0.000	0.000	0.000	0.000	0.000
Mn^{2+}	0.067	0.070	0.001	0.001	0.001	0.056	0.000
Fe^{3+}	0.829	0.825	0.221	0.172	1.386	0.823	0.058
Sum	2.838	2.834	2.075	2.024	3.791	2.827	1.878

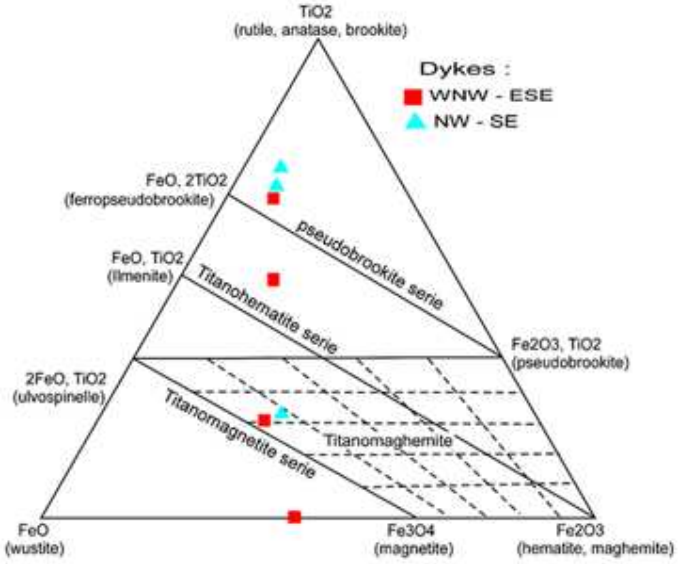

Figure 8: Mineralogical composition of Fe-Ti oxides from the doleritic dykes in the Ayorou and Kandadji areas, plotted on the FeO–Fe_2O_3–TiO_2 diagram (Deer et al., 1969).

5. Discussion

5.1. Petrography and alteration process of Fe-Ti-V oxide mineralizations

Field observations show that the Fe-Ti-V oxide mineralizations of our study area occur at outcrop as alteration patinas of Fe-Mg minerals along the chilled margins and fragmented blocks at the centers of doleritic dykes. In thin sections, these mineralization appear in a crystallized oxides, as granular aggregates of titanomagnetites containing bands of ilmenite. This lattice texture is characteristic of high-temperature deuteric oxidation, during which ilmenite exsolutions crystallized into titanomagnetites under the influence of aqueous magmatic fluids. The process continued at low temperatures, leading to the transformation of the crystals margins of titanomagnetites into titanomaghemites, with the partial disappearance of the ilmenite bands. This high-temperature deuteric oxidation is associated with deuteric alteration during which ferroedenite recrystallized at the margins of augite crystals, in according with the hypothesis formulated by Noura et al. (2023a) to explain the evolution of mineral phases in these dykes. The transformation of titanomagnetites into titanomagnetites was explained by Pivot et al. (1968), who supposed that it involves a decrease in Fe content and an increase in Mn and Ti concentrations during its formation. For other authors (e.g., Ondrejka et al., 2015), this transformation occurs during the maghemite formation mechanism, which results from deuteric oxidation at low temperatures, generally below 150°C (Ozdemir and Moskowitz, 1992). This temperature is relatively higher in the results highlighted in this study, reaching 200°C as shown in Figure 10b. During this mechanism, the aqueous fluids at the end of crystallization acted on the margins of titamagnetite crystals by transforming Fe^{2+} into Fe^{3+} ion, with a slight enrichment in Mn and Ti (Figure 9a). According to Xu et al. (1997), the maghemite formation mechanism consists of Fe^{2+} ion migration through solid diffusion toward the surface or exterior of the titanomagnetite crystal, without the addition of oxygen. Based on the alteration, it is noted that these mineralizations are associated with silicate minerals such as hornblende and chlorite, within which the amount of Fe can be relatively significant, but also with titanomaghemites that are enriched in Mn and Ti from the titanomagnetites (Table 2).

The lattice and granular textures identified in this study, which are typical of high-temperature titanomagnetite oxidation, are similar to the ilmenite lamellae included in titanomagnetite described in the Panzhihua mafic intrusion in China (Dankali, 2016) and in the Fedorivka layered intrusion (Duchesne et al., 2006), and were interpreted by Charlier et al. (2015) as ilmenite exsolutions from magnetite during the oxidation of ulvospinel component, producing ilmenite lamellae above the magnetite-ulvospinel solvus.

5.2. Origin and formation conditions of Fe-Ti-V oxide mineralizations

Fe-Ti-V oxide mineralizations may have a primary origin directly linked to syn- to late-magmatic processes or a secondary origin linked to post-magmatic processes. Several hypotheses have been proposed to explain the origin and formation conditions of Fe-Ti-V oxide mineralizations, ranging from magmatic crystallization (e.g., Karinen et al., 2022) to hydrothermalism (e.g., Li et al., 2014; Dare et al., 2015), to deuteric oxidation (Ondrejka et al., 2015) and/or supergene alteration (e.g., Weibel, 2003). Other authors propose alternative mechanisms, notably liquid immiscibility (Reynolds et al., 1985; Bachari, 2004; Charlier et al., 2015) and magma mixing or

contamination (Harney et al., 1990). Most of these processes and mechanisms have been reported by Noura et al. (2023a), who demonstrated an asthenospheric origin for the doleritic dykes of the Téra-Ayorou pluton, whose magma underwent various degree of crystallization between the margins and centers of the dykes, accompanied by deuteric alteration responsible for the recrystallization of ferro-edenite and hydrothermal alteration forming chlorite. The physical characteristics of the oxidized minerals in thin sections and the sample projection in oxide diagrams (Figures 8 and 9) suggest that at least two mechanisms contributed to the formation of Fe-Ti-V mineralizations observed in high-resolution SEM images or through the electron microprobe analysis results of titanomagnetite, sulfides, titanomaghemite and ilmenite. Thus, these mineralizations formed in the form of: (*i*) Fe during surface fluvial weathering, (*ii*) Fe-Ti during fractional crystallization of clinopyroxenes, recrystallization of hornblende during deuteric alteration, and Fe-Ti-V during: (*iii*) fractional crystallization of titanomagnetite-ilmenite-ulvospinel and (*iv*) low-temperature recrystallization of titanomaghemite. The deuteric nature of the oxidation is shown by the presence of titanomaghemite, as demonstrated some samples projection in the FeO-Fe_2O_3-TiO_2 diagram (Ondrejka et al., 2015), within the titanomaghemite field during deuteric oxidation (Figure 10). Electron microprobe analyses (Table 2), chemical maps (Figure 7a, b, c, d, e, f), and SEM images (Figure 7g, h) results, appear that the potential sources of these mineralizations are oxidized minerals (titanomagnetite, ilmenite and titanomaghemite) and, to a lesser extent, ferric silicate minerals (chlorite, augite, hornblende) and metal sulfides (pyrite, chalcopyrite). In order to understand the minor contribution of hydrothermal alteration affecting plagioclase and hornblende in this study, Charlier et al. (2015) proposed that this process reduces the Fe and Ti contents in oxides, by integrating plagioclase elements (i.e., Ca in this study) in their crystal structure.

Through studies of magma evolution during fractional cristallisazation, several works on mineral migration within magma chamber have concluded that oxidized minerals, due to their high density, tend to migrate toward the bottom of the magma chamber, and that the crystallization and precipitation of minerals such as titanomagnetite and ilmenite are largely controlled by oxygen fugacity (Charlier et al., 2015), magma temperature (Hill and Roedder, 1974), the Fe, Ti, V contents of magma (Bachari, 2004), and pressure variations (Cawthorn et al., 1985). It is accepted that during magma crystallization, ilmenite coexists with magnetite, and the two oxides are linked through a cation exchange between $Fe^{2+}Ti^{4+}$ and Fe^{3+}, during which magnetite gets Fe^{3+} and ilmenite obtains $Fe^{2+}Ti^{4+}$ (Duchesne, 1972; Charlier et al., 2015), to form titanomagnetite with internal growth of ilmenite bands and ulvospinelle grains. These process are accompanied by the addition of Mn at low temperature, from the residual liquid, in addition to the acquisition of $Fe^{2+}Ti^{4+}$ through the chemical reaction $3Fe_2TiO_4 + 1/2O_2 \rightarrow 3FeTiO_3 + Fe_3O_4$, to form titanomaghemite. These hypothesis explain essentially the condition formation of oxide minerales and Fe-Ti-V oxide ores of our study area.

The presence of relatively high contents of Ca in these mineralizations is linked to the vanadium-bearing nature of titanomagnetite and could be explained by several mechanisms as demonstrated: (*i*) the incorporation of Ca in titanomagnetite from silicate minerals such as clinopyroxene or ca plagioclase, (*ii*) the crystallization of Ca at the margins of titanomagnetite crystals from magmatic fluids resulting from deuteric alteration, (*iii*) the presence of fine perovskite intergrowths within titanomagnetite formed from a magma Ca-rich, or (*iv*) through very slight isomorphic substitution of Ca in the interstitial space or defects in the spinel crystal lattice. All of these process, with the exception of the first and last one (because Ca cannot substitute for Fe), could explain the presence and abundance of Ca content in these mineralizations.

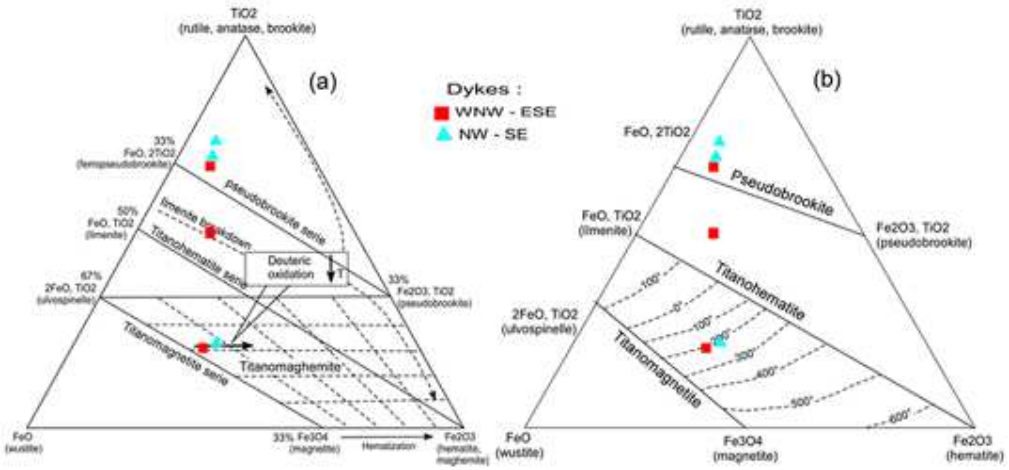

Figure 10: FeO-Fe_2O_3-TiO_2 ternary diagram (Ondrejka et al., 2015).

6. Conclusion

The Fe-Ti-V oxide mineralizations of the Téra-Ayorou pluton origenated from asthenospheric and formed during fractional crystallization in the titanomagnetite, sulfides and clinopyroxenes, deuteric alteration in titanomagnetite and hornblende, and hydrothermal alteration in chlorite. Among these elements, Ti and Fe concentrations are predominant and occur in all minerals, unlike V, which is found in trace amounts and is predominantly present in titanomagnetite, ilmenite, and titanomaghemite. The evolution of mineral phases from titanomagnetite to titanomagnetite is accompanied by a slight enrichment in Ti and Mn at the margins and the disappearance of ilmenite bands, reflecting low-temperature deuteric oxidation. The high TiO_2 contents in ilmenite, titanomagnetite, and titanomaghemite compared to clinopyroxenes is explained by their late crystallization and the low fractionation of Ti during the early formed crystals such as clinopyroxenes. The presence of Ca in vanadiferous titanomagnetite and in its residual product (titanomaghemite), reflects the incorporation of Ca into their crystal structure during high-temperature deuteric alteration or oxidation. It would be important to develop this work by integrating fluide inclusion, thermobarometry and U-Pb geochronological analyses, in order to determine the age of these mineralizations, the P-T emplacement conditions, to assess their petrogenetic model.

Acknowledgments

Authors thank Mr. Mohamed Pegnalogo Ouattara of the UDR STRM laboratory at Félix-Houphouët Boigny University (Ivory Coast) for preparing the thin sections, and Dr. Philippe Parseval of the GET laboratory at the University of Toulouse (France) for the microprobe analyses and chemical mapping.

Reference

[1] Abass Saley, A., Baratoux, D., Baratoux, L., Ahoussi, K. E., Yao, K. A., Kouamé, K. J. (2021). Evolution of the Koma Bangou Gold Panning Site (Niger) From 1984 to 2020 Using Landsat Imagery. Earth and Space Science, 8, e2021EA001879. 1-25.

[2] Aïfa, T. (2021). Mineralization and Sustainable Development in the West African Craton: From Field Observations to Modelling. Geological Society. London. Special Publications. 502, 1–29.

[3] Ahmed, Y., Attourabi, S.A., Hallarou, M.M., Chamsi, L.I., Noura, G.R. and Sanda, C.M.M. (2022). Relationship between Regional Deformation and the Emplacement of the Dibilo Pegmatites (Liptako, West Niger). Journal of African Earth Sciences,198, Article ID: 104814.

[4] Ama Salah, I., Liegeois, J.P. and Pouclet, A. (1996). Évolution d'un arc insulaire océanique birimien précoce au Liptako nigérien (Sirba): Géologie, géochronologie et géochimie. Journal of African Earth Sciences. 22, 235-254.

[5] Ama Salah, I. (1991). Pétrographie et relations structurales des formations metavolcaniques et sédimentaires du Birimien du Niger occidental. Problème de l'accrétion crustale au paléoprotérozoique inférieur. Ph.D. Thesis, Université d'Orléans, Orléans.

[6] Attourabi, S., Marieke, V. L., Hallarou, M. M., A., Ahmed, Y., Mamane Moustapha. S., C. (2024b). Petrogragenetic realtionships between paleoproterozoic granitoids and rare-element pegmatites from Dibilo (Liptako, West Niger, West African Craton). Journal of African Earth Sciences. 220, 105440.

[7] Bachari, H. (2004). La genèse des dépôts d'oxydes fer, titane et vanadium associés aux anorthosites massives de la région de lac-saint-jean (saint-charles et lac élan) et de la région de havre saintpierre (massif de la rivière-au-Tonnerre, massif de la rivière Romaine et massif de Lac Allard), québec, Canada. Mémoire de Master. 167p.

[8] Bai, Z. J., Zhong, H., Zhu, W. G., Hu, W. J., Chen, C.J. (2019). The genesis of the newly discovered giant Wuben magmatic Fe–Ti oxide deposit in the Emeishan Large Igneous Province: A product of the late-stage redistribution and sorting of crystal slurries. Miner. Depos. 54, 31–46.

[9] Ballo, I., Hein, K. A. A., Guindo, B., Sanogo, L., Ouologuem, Y., Daou, G. and Traore, A. (2015). The Syama and Tabakoroni Gold Fields, Mali. Ore Geology Reviews. 78, 578-585.

[10] Baratoux L, Metelka V, Naba S, Jessell MW, Grégoire M, Ganne J. (2011). Juvenile Paleoproterozoic crust evolution during the Eburnean orogeny (~2.2-2.0Ga), western Burkina Faso. Precambrian Res. 191. 18–45.

[11] Béziat, D., Dubois, M., Debat, P., Nikie, S., Salvi, S. and Tollon, F. (2008). Gold Metallogeny in the Birimian Craton of Burkina Faso (West Africa). Journal of African Earth Sciences. 50, 215-233.

[12] Baratoux, L., Jessell, M. W., Kouamelan, A. N. (2024). The West African Craton. 3, 48–68.

[13] Charlier, B., Namur, O.; Bolle, O., Latypov, R., Chesne, J.-C. (2015). Fe-Ti-V-P Ore deposits associated with Proterozoic massif-type anorthosites and related rocks. Earth Sci. Rev., 141, 56–81.

[14] Cao, J. Wang, X., Tao., J. (2020). Petrogenesis of the Piqiang mafic-ultramafic layered intrusion and associated Fe-Ti-V oxide deposit in Tarim Large Igneous Province, NW China. 10-13, 1-38.

[15] Cawthorn, R.G.; McCarthy, T.S. (1985). Incompatible trace element behavior in the Bushveld Complex. Econ. Geol. 80, 1016–1026.

[16] Dankali, I. M. (201). Origine des oxydes de Fe-Ti-V de la partie basale de l'intrusion de Panzhihua, SW de la Chine. Mémoire de Master. 61p.

[17] Dare, S. A .S., Barnes, S.-J., Beaudoin, G., Méric, J., Boutroy, E., Potvin-Doucet, C. (2014). Trace elements in magnetite as petrogenetic indicators. Miner. Depos. 49, 785–796.

[18] Deer, W. A., Howie, R. A., Zusmam, J. An introduction to the rock-forming minerals. First edition. 506p.

[19] Duchesne, J.C., Shumlyanskyy, L., Charlier, B. (2006). The Fedorivka layered intrusion (Korosten Pluton, Ukraine): an example of highly differentiated ferrobasaltic evolution. Lithos. 89, 353–376.

[20] Duchesne, J.C. (1972). Iron–titanium oxide minerals in the Bjerkrem–Sogndal Massif, South-western Norway. J. Petrol. 13, 57–81.

[21] Dupuis D., Pons J., Prost A. E. (1991). Mise en place de plutons et caractérisation de la déformation au Niger Occidental. CR Acad Sci Paris, t.309, 816 Série ll, 1847–1853.

[22] Ennih, N., Li´egeois, J. P. (2008). The boundaries of the West African craton, with special reference to the basement of the Moroccan metacratonic Anti-Atlas belt. Geol. Soc. Spec. Publ. 297 (June), 1–17.

[23] Garba Saley, H., Konaté, M., Okunlola, O. A. (2024). Petrographic Study of Mn-bearing Gondite (Birimian) of Téra Area in the Leo-Man Shield (West African Craton) in Niger. Economic and Environmental Geology. 57, 25–39.

[24] Flaknazi, M., & Karimi, M. (2014). The Mineralization of Titanium and Iron in Gabbros of Ophiolitic Fanouj Zone, Sistan & Baluchestan, Iran. Journal of Biodiversity and Environmental Sciences. 5, 432-440.

[25] Grenholm M, Jessell, M., Thébaud, N. (2019). Ageodynamicmodel for the Paleoproterozoic (ca.2.27–1.96Ga)BirimianOrogen of the southern West African Craton: Insights into an evolving accretionarycollisional orogenic system. Earth-Sci Rev, 192. 138–193.

[26] Gloaguen, E., Augé, T., Bailly, L., Courrioux, G., Fullgraf, T., Perrin, G. (2015). A new type of large ultramafic intrusion-hosted Fe-Ti-V deposit in the West-African Archean Craton: The N'Guérédonké complex, Guinea. Bureau de Recherche Géologique et Minière (BRGM). 4p.

[27] Hallarou, M. M., Konaté, M., Olatunji, A. S., Ahmed, Y. (2020b). The Kourki porphyry Cu-Mo deposit is located in the southern part of the Gorouol greenstone belt in Western. Geological Society, London, Special Publications. 1, 1–13.

[28] Harney, D. M. W., Merkle, R. K. W., Von Gruenewaldt, G. (1990). Platinum-group element behavior in the lower part of upper zone, eastern Busheved Complex; implication for the formation of the main magnetite layer. Econ. Geol. 85, 1777-1789.

[29] Hill, R., Roedder, P. L. (1974). The crystallisation of spinel from basaltic liquide as a fonction of oxygen fugacity. Journal of Geology. 82, 709-729.

[30] Ibrahim Maharou, H. Laouali Idi, K., Alzouma Amadou, D., Ganiou Amadou, S. A. (2024a). Exoscopy of detrital zircon from Niamey Sandstones (Eastern edge of the West African Craton, Southwestern Niger). Interpretation of detrital sediments provenance, Open Journal of Geology. 14, 617-628.

[31] Jessell, M., Santoul, J., Baratoux, L., Youbi, N., Ernst, R.E., Metelka, V., Miller, J., Perrouty, S. (2015). An updated map of West African mafic dykes. J. Afr. Earth Sci. 112, 440–450.

[32] Jiang, M., Liu, W., Zu, B., and Wang, W. (2024). Formation of Ferrogabbro Through Fe-Ti Oxide Accumulation Under Moderate Oxidation Conditions: Insights from the

Dashanshu Intrusion in the Emeishan Large Igneous Province, SW China. Minerals, 14, 1156.

[33] Jonsson, E., Troll, V. R., Högdahl, K., Harris, C., Weis, F., Nilsson, K. P., Skelton, A. (2013). Magmatic origin of giant 'Kiruna-type' apatite-iron-oxide ores in Central Sweden. Sci Rep 3, p1644.

[34] Karinen, T., Moilanen, M., Kuva, J., Lahaye, Y., Datar, B. & Yang, S. (2022). Mustavaara revisited: A revised genetic model for orthomagmatic Fe–Ti–V mineralisation in the Koillismaa intrusion. Geological Survey of Finland, Bulletin 414, 49 pages, 31 figures, 2 tables, 19 appendices and 3 electronic folders including raw data.

[35] Khalil, K., Summers, P., El Shazly, A. (2023). Origin of the post collisional younger gabbroic rocks and the associated Fe–Ti oxide ores, Abu Ghalaga area, Southern Eastern Desert, Egypt: Mineralogical and geochemical constraints. Arab. J. Geosci. 16, 160.

[36] Khedr, M. Z., Takazawa, E., Arai, S., Stern, R.J., Morishita, T., El-Awady, A. (2022). Styles of Fe–Ti-V ore deposits in the Neoproterozoic layered mafic-ultramafic intrusions, South Eastern Desert of Egypt: Evidence for fractional crystallization of V-rich melts. J. Afr. Earth Sci. 194, 104620.

[37] Kouamelan, A. N, Kra, K. S. A, Djro, S. C, Paquette, J. L, Peucat, J. J. (2018). The Logoualé Band: A large Archean crustal block in the Kenema-Man domain (Man-Leo rise, West African Craton) remobilized during Eburnean orogeny (2.05 Ga). J. Afr. Earth Sci. 148, 6–13.

[38] Latypov, R. M., Namur, O., Bai, Y., Barnes, S. J., Chistyakova, S. Y., Holness, M. B., Iacono-Marziano, G., Kruger, W. A. J., O'Driscoll, B., Smith,W. D., et al. (2024). Layered intrusions: Fundamentals, novel observations and concepts, and controversial issues. Earth-Sci. Rev. 249, 104653.

[39] Li, H., Li, L., Zhang, Z., Santosh, M., Liu, M., Cui, Y., Yang, X., Chen, J., Yao, T. (2014). Alteration of the Damiao anorthosite complex in the northern North China Craton: implications for high-grade iron mineralization. Ore Geol. Rev. 57, 574–588.

[40] Lompo, M. (2009). Geodynamic evolution of the 2.25-2.0 Ga Palaeoproterozoic magmatic rocks in the Man-Leo shield of the West African Craton. A model of subsidence of an oceanic plateau. Geol Soc Spec Publ. 323, 231–254.

[41] Machens, E. (1973). Contribution à l'étude des formations du socle cristallin et de la couverture sédimentaire de l'Ouest de la République du Niger. Mémoire du BRGM, Paris.

[42] Markwitz, V., Hein, K. A. A., Jessell, M. W., Miller, J. (2016). Metallogenic portfolio of the West Africa Craton. Ore Geology Rewiews. 78, 558-563.

[43] Mohammad, A., Prasad, A. K., Wetsah, K., Azad, M., Aryan, V. and El-Askary, H. (2022). Titaniferous-Vanadiferous, Magnetite-Ilmenite Mineralization in a Mafic Suite within the Chhotanagpur Gneissic Complex, Bihar, India. Minerals 2022, 12, 860.

[44] Noura, G . R., Baratoux, L., Ernst, R. E., El Bilali, H., Abass Saley A. L., Hantchi, K. D., Bohari A. D., Ahmed Y. (2025). Mineralogical and geochemical characteristics of the NNW-NNE trending Libiri doleritic dyke swarm of the Paleoproterozoic Liptako basement (West Niger): Genesis and magmatic evolution, BSGF - Earth Sciences Bulletin 196: 18. 1-23.

[45] Noura, G. R., Tourba, K., Hantchi, K. D., Hassane, B., Konaté, M. (2024). Characteristics of gold and its mineralization style in the Boulon Djounga Eastern perimeter of Liptako Mining Company (Central Southwestern Niger). Natural Resources, 2024, 15, 28-50.

[46] Noura, G. R., Ahmed, Y., Hallarou, M. M., Maharou, H. I., & Abdourahamane, S. (2023b). Structural characteristics of the granitoids in the Ayorou and Kandadji area (Liptako, western Niger). International Journal of Innovation and Applied Studies 40, 1423–1436.

[47] Noura G. R, Ahmed, Y., Baratoux, L., Ernst, R. E., Attourabi, A. S., Hallarou, M. M., Chamsi, L. I., Chékaraou, M. M. S. (2023a). Petrogenesis and geochemistry of WNW-ESE to NW-SE trending doleritic dykes of the Paleoproterozoic Liptako basement (West African Craton, West Niger). J Afr Earth Sci 208: 1–17.

[48] Ondrejka, M., Broska, I., Uher, P. (2015). The late magmatic to subsolidus T-fO2 evolution of the Lower Triassic A- type rhyolites (Silicic Superunit, Western Carpathians, Slovakia): Fe–

Ti oxythermometry and petrological implications. acta geologica slovaca, 7(1), 51–61.

[49] Ousmane, H., Hantchi, K. D., Hamidou, L.B., Ali, I. A. and Konaté, M. (2020). Caractérisation de la déformation des dépôts oligocènes du Continental terminal 3 (Ct^3) dans la région de Niamey (Bordure Orientale du Craton Ouest Africain, Bassin des Iullemmeden). European Scientific Journal , 16, 418-441.

[50] Ozdemir, O., Oreilly, W. (1982), An experimental study of thermoremanent magnetization acquired by synthetic monodomain titanomaghemites, Journal of Geomagnetism and Geoelectricity. 34, 467-478.

[51] Pang, K. N., Zhou, M. F., Qi, L., Shellnutt, J. G., Wang, C. Y., Zhao, D. G. (2010). Flood basalt-related Fe-Ti oxide deposits in the Emeishan large igneous province, SW China. Lithos, 119, 123–136.

[52] Parra-Avila, L. A., Kemp, A. I. S., Fiorentini, M. L., Belousova, E., Baratoux, L., Block, S., et al. (2017). The geochronological evolution of the Paleoproterozoic Baoulé-Mossi domain of the Southern West African Craton. Precambrian Res 300, 1–27.

[53] Pivot, M., Rémond, G., Caye, R. (1968). Etude de la transformation d'une titanomagnétite en titanomaghémite dans une roche volcanique. Bulletin de minéralogie. 91, 65-74.

[54] Pons, J., Barbey, P., Dupuis, D. and Léger, J.M. (1995). Mechanisms of Pluton Emplacement and Structural Evolution of a 2.1 Ga Juvenile Continental Crust: The Birimian of Southwestern Niger. Precambrian Research , 70, 281-301.

[55] Reynolds, I. M. (1985). The nature and origin of titaniferous magnetite-rich layers in the upper zone of the Bushveld complex: A review and synthesis: Economic Geology, v. 80, p. 1089–1108.

[56] Sangaré, A., Driouch, Y., Salvi, S. and Al, E. (2014). Geology of Kalana late-Eburnean Gold Deposit (Birimian, Southwestern Mali). Bulletin de l'institut Scientifique: Rabat, Section Sciences de la Terre. 1, 85-108.

[57] Song X. Y., Qi, H. W., Hu, R. Z., Chen, L. M., Yu, S. Y., Zhang, J. F. (2013). Formation of thick stratiform Fe-Ti oxide layers in layered intrusion and frequent replenishment of fractionated mafic magma: evidence from the Panzhihua intrusion, SW China. Geochem Geophys Geosyst. 14, 712–732.

[58] Soumaila, A., Garba, Z., Moussa, I.A., Nouhou, H. and Sebag, D. (2016). Highlighting the Root of a Paleoproterozoic Oceanic arc in Liptako, Niger, West Africa. Journal of Geology and Mining Research. 8, 13-27.

[59] Soumaila, A., Henry, P., Garba, Z. and Rossi, M. (2008). REE Patterns, Nd-Sm and U-Pb Ages of the Metamorphic Rocks of the Diagorou-Darbani Greenstone Belt (Liptako, SW Niger): Implication for Birimian (Palaeoproterozoic) Crustal Genesis. Geological Society. 297, 19-32.

[60] Soumaila, A., Konaté, M. (2005). Caractérisation de la déformation dans la ceinture birimienne (paléoprotérozoique) de Diagorou-Darbani (Liptako nigérien, Afrique de l'Ouest). Africa Geoscience Review. 12, 161-178.

[61] Thiéblemont, D., Goujou, J. C., Egal, E., Cocherie, A., Delor, C., Lafon, J. M., et al. (2004). Archean evolution of the Leo Rise and its Eburnean reworking. J Afr Earth Sci 39: 97–104.

[62] Uwamungu, P., Chen, W., Zhao, X., Zhao, K., Jiang, S. (2023). Evolution of Fe-Ti oxides within the Tiechagou carbonatite-related iron deposit: Insights from texture and in situ chemical compositions of magnetite and ilmenite. Ore Geology Reviews 157, 105439.

[63] Vidal, M., Gumiaux, C., Cagnard, F., Pouclet, A., Ouattara, G. and Pichon, M. (2009). Evolution of a Paleoproterozoic "Weak Type" Orogeny in the West African Craton (Ivory Coast). Tectonophysics , 477, 145-159.

[64] Weibel, R. (2003). Alteration of detrital Fe-Ti oxides in Miocene fluvial deposits. central Jutland. Denmark. Bulletin of the Geological Society of Denmark. 50, pp. 171–183.

[65] White, A., Burgess, R., Charnley, N., Selby, D., Whitehouse, M., Robb, L. and Waters, D. (2014). Constraints on the Timing of Late-Eburnean Metamorphism, Gold Mineralisation and Regional Exhumation at Damang Mine, Ghana. Society of Economic Geologists , 1, 1009-1025.

[66] Xu, W. X., Peacor, D. R., Dollase, W. A., Van Der Voo, R., Beaubouef, R., (1997). Transformation of titanomagnetite to

titanomaghemite: A slow, two-step, oxidation-ordering process in MORB, American Mineralogist, 82(11-12), 1101-1110.

[67] Youbi, N., Ernst, R., Söderlund, U., Bertrand, H., Doblas, M., El Hachimi, H., et al. (2011). Large igneous provinces of the West African Craton: The record preserved in regional dyke swarms. Large Igneous Provinces Commision, May, 1–12.

[68] Zhou, M. F., Chen, W. T., Wang, C. Y., Prevec, S. A., Liu, P. P., Howarth, G. H. (2013). Two stages of immiscible liquid separation in the formation of Panzhihua-type Fe-Ti-V oxide deposits, SW China. Geosci. Front. 4, 481–502.